

Supporting information for Caesium incorporation and retention in illite interlayers

Adam J. Fuller, Samuel Shaw, Michael B. Ward, Sarah J. Haigh, J. Frederick W. Mosselmans, Caroline L. Peacock, Stephen Stackhouse, Andrew J. Dent, Divyesh Trivedi and Ian T. Burke*

*Corresponding author e-mail: i.t.burke@leeds.ac.uk

S1. Extended Materials and Methods

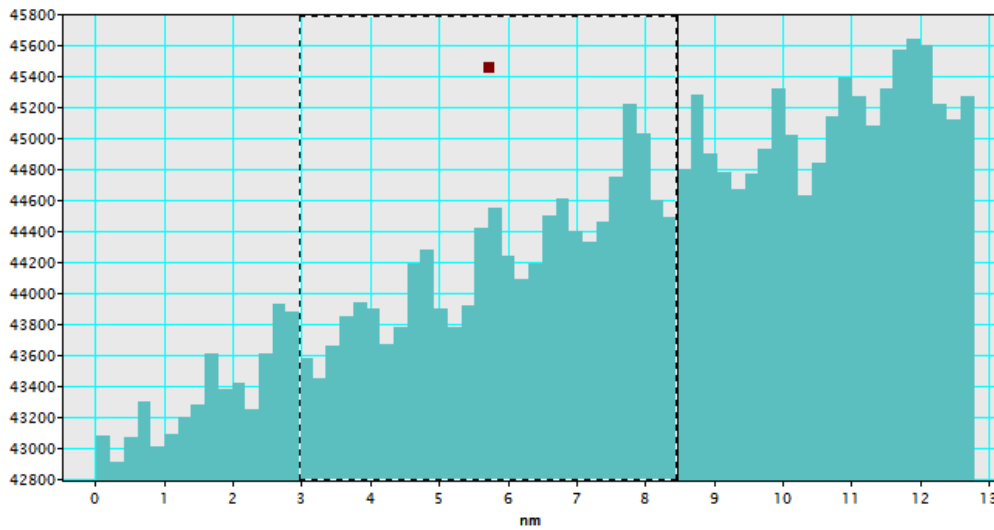


Fig. S1 Representative histogram of image contrast used to determine layer spacings presented in Fig. 2e. Each peak represents an area of higher intensity (a TOT layer) and each trough, lower intensity (a K interlayer).

S2. Negative control sample: Illite suspended in deionised water for 4 months

A large section of our work relies on the assumption that all compositional changes result from the presence of the ions in solution and there is negligible release of K from the illite interlayer due to equilibration with aqueous solution (deionised water). Additionally we assumed that any release did not cause a change in the layer thickness. To confirm this assumption and disprove the null hypothesis we equilibrated our starting illite material with deionised water for 4 months. The samples were then imaged to determine any change in layer spacing and analysed by energy dispersive x-ray (EDX) spectroscopy to quantify any loss of K. Figure S1 shows the two EDX spectra from the starting illite material and from the sample exposed to deionised water for 4 months. We normalised the data on the silicon peak and determined the K/Si ratio for both systems. The starting illite material had a K/Si ratio of 0.19 and the K/Si ratio of illite after equilibration with deionised water was also 0.19. From this we can confirm that any loss of K into solution was negligible and cannot account for the large reduction in K seen in data from both our Ca and Cs exposed systems. When the crystal structure of the illite material suspended in deionised water was imaged we found no evidence of edge fraying or expansion (Fig. S2). We therefore assert that the expansion seen in the Ca and Cs systems must be due to the sorption of hydrated Ca or Cs ions rather than just a loss of K.

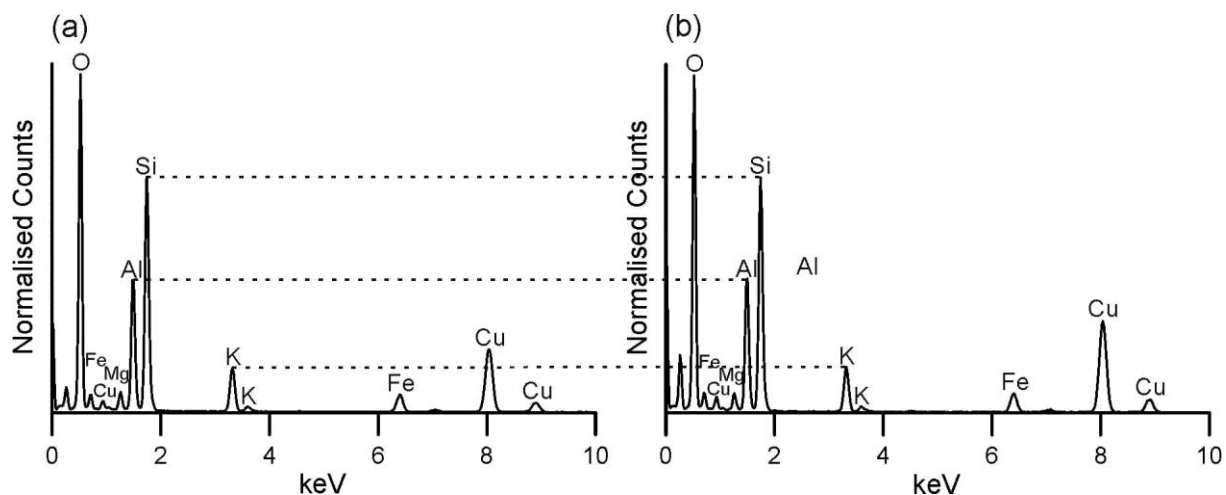


Figure S2 Energy dispersive x-ray spectra of (a) the starting illite material and (b) illite suspended in deionised water for 4 months. Spectra are normalised to the Si peak and show no difference in concentrations of Al or K. The Cu peak at 8 keV is from the support grid and unrelated to the sample's composition.

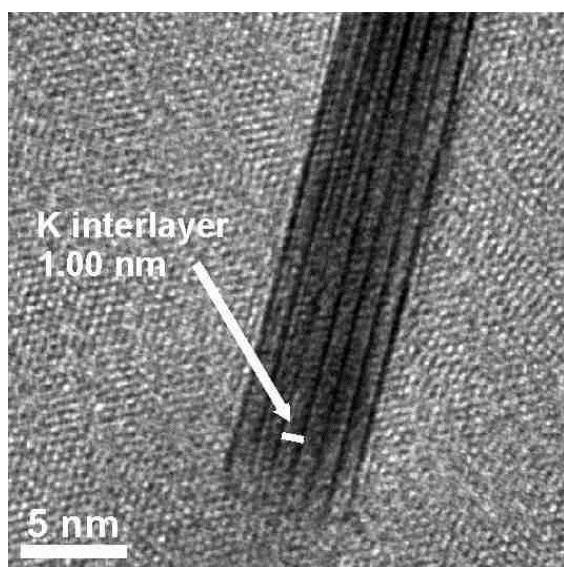


Figure S3 Starting illite material suspended in deionised water for 4 months shows no presence of frayed edges

S3. Ca illite EDX

In the main text we made the assertion that the change in layer thickness seen in figure 1 was due to the exchange of Ca and Cs into the edge interlayer spaces. Here we present EDX spectra from flakes from within the same sample as is imaged in figure 1. It should be noted that due to beam damage constraints it was not possible to both image and perform EDX analysis on the same flakes. However the assumption is made that there was uniform ion exchange within the interlayers of all flakes in the sample. Although attempts were made to gather data on the atomic composition at the edge of the crystal the very low concentrations meant that this was only possible in the case of the Ca-illite (Fig. S3b) and the Ca suspended Cs illite (Figure S3d). EDX spectra for the starting material (Figure S3a) and the Cs illite (Figure S3c) were gathered from a bulk crystal. Therefore, these latter two samples have a much improved signal to noise ratio. Spectra b and d are cropped at 8keV to remove the large Cu peak caused by their close proximity to the copper grid.

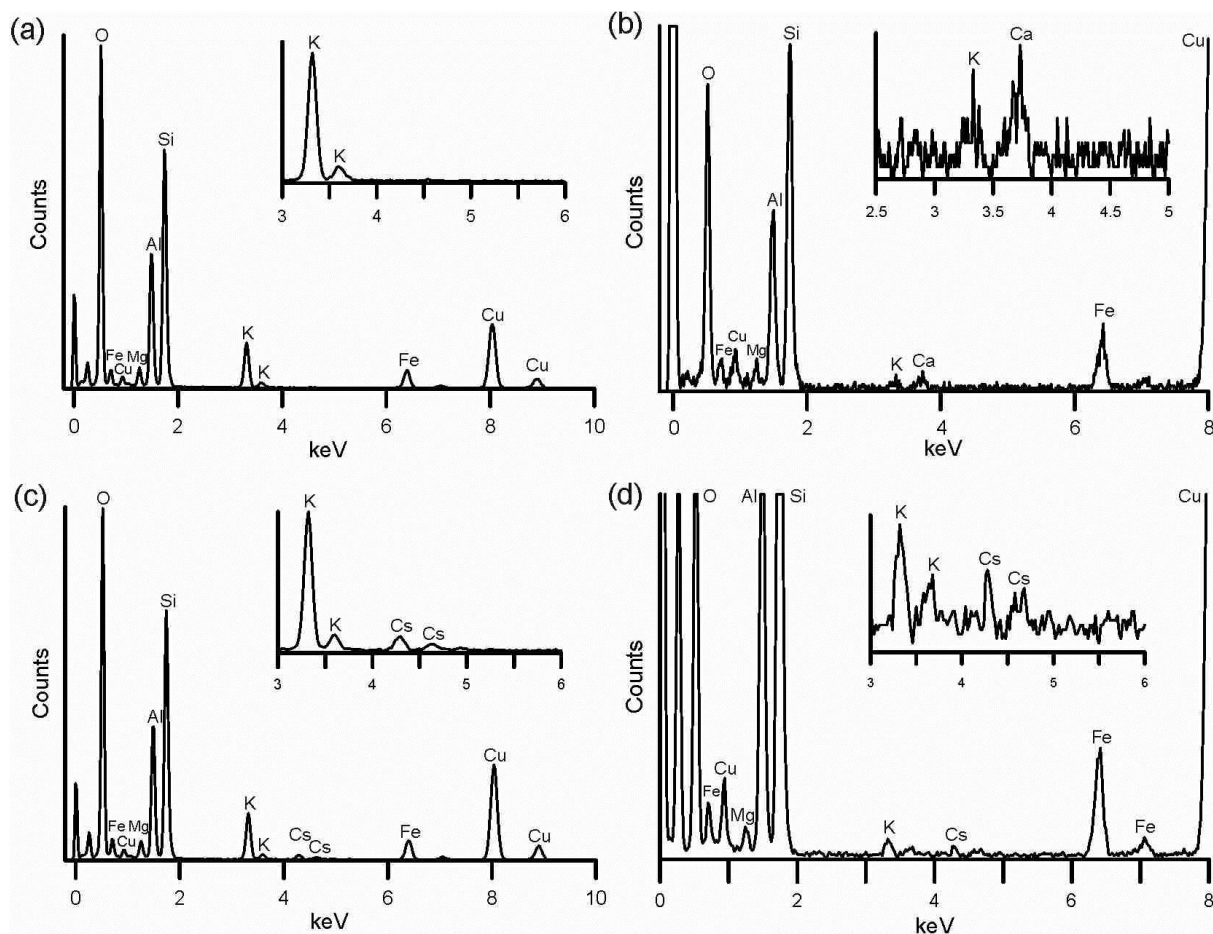


Figure S4 EDX spectra associated with the Ca/Cs illite series (main text figure 1). (a) Starting illite material, for which no Ca K_{α} peak at 3.7 keV or Cs L_{α} peak at 4.3 keV are observed to be present, (insert shows enlargement of relevant region between 3 and 6 keV). (b) Ca illite showing Ca peak at 3.7 keV, insert shows an enhancement of the region with the Ca peak. (c) Cs exchanged Ca-illite shows loss of Ca peak and presence of Cs L_{α} peak at 4.3 keV, showing that Cs has exchanged for Ca in the illite structure. (d) Interlayer remains Cs filled and shows no Ca present, even after suspension in 0.1 mol L^{-1} CaCl.

S4. Long term sorption EDX

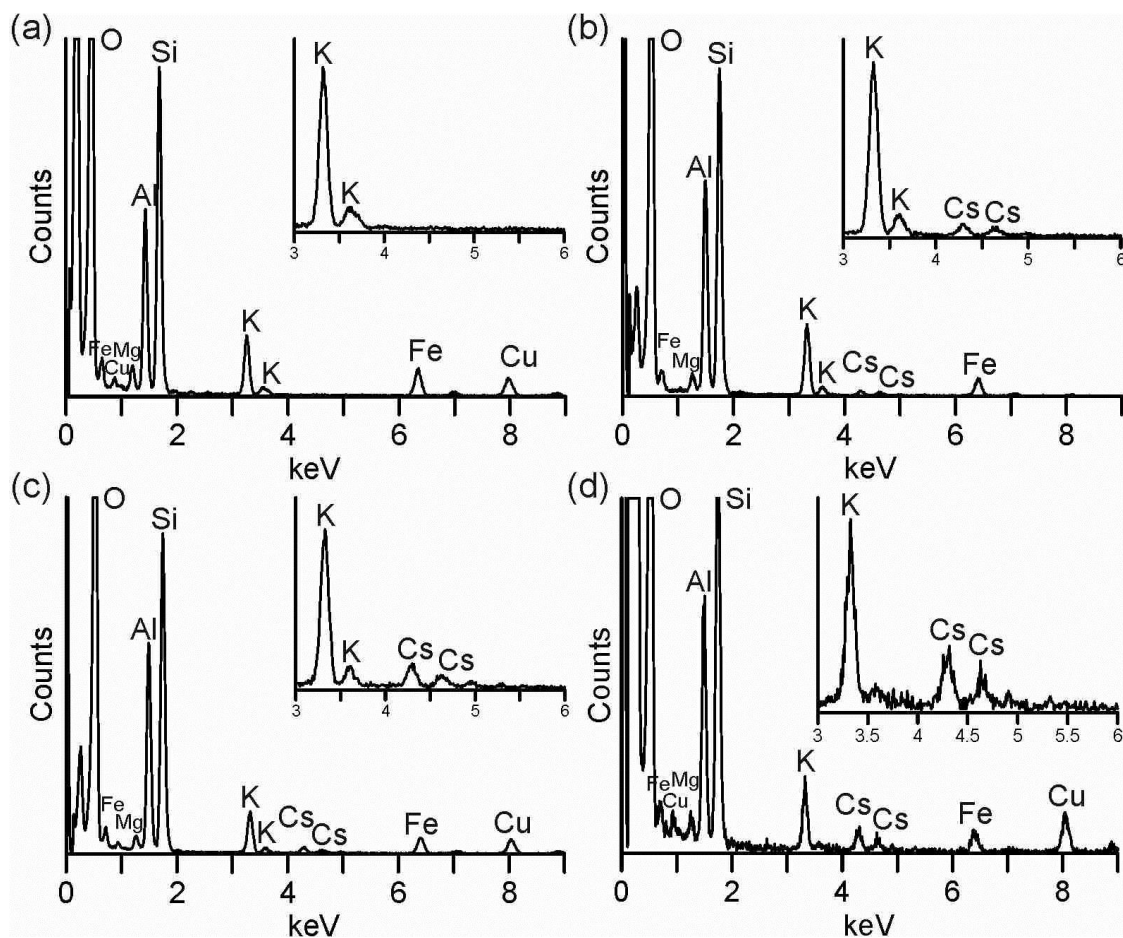


Figure S5 EDX spectral composition of (a) illite starting material, before Cs exposure (b) illite suspended in Cs for 4 months (c) illite suspended in Cs for 7 months (d) illite after 1 year of Cs exposure.

Table S1 Atomic percentage composition of the different elements in the illite after suspension in Cs for up to 1 year; measured through semi-quantitative analysis of the EDX spectra presented in Fig S4.

Elements	Starting illite / atomic %	4 months / atomic %	7 months / atomic %	12 months / atomic %
O	58	52	54	49
Si	21	23	23	24
Al	11	14	14	13
Cs	0	2	2	6
K	5	6	4	5
Fe	3	3	2	3
Mg	1	1	1	1
Na	0	0	0	0

S5. Density Functional Theory (DFT) analysis of illite structure

We used a density function theory model to determine the theoretical change in the illite layer thickness from substitution of interlayer K for Cs. From this we determined a change in layer thickness that was consistent with the average change measured in the TEM images. The full lattice parameters and layer-spacings are presented in table S3 and shown graphically in figure 3b of the main text. The calculations were performed using both local density approximation (LDA) (Perdew and Zunger, 1981) and PBE formulation of the generalized gradient approximation (GGA) (Perdew et al., 1996). The results show a 0.5Å difference in the overall layer-spacing calculated by these two approximations. However the extent of expansion predicted when the interlayer K was replaced by Cs was the same in both methods, and was also consistent with the measured interlayer expansion (main text Figure 2).

Table S2 Lattice parameters for a K and Cs substituted illite based on both the local density and generalised gradient approximations. In both cases lattice parameters for two different configurations of isomorphic substitution are given.

Local Density Approximation							
Interlayer cation	Cell length			Cell angle			Illite layer thickness (Å)
K	a (Å)	b (Å)	c (Å)	α (degrees)	β (degrees)	γ (degrees)	
Substitution 1	10.32	8.906	9.969	89.504	102.094	89.823	9.747
Substitution 2	10.319	8.912	9.965	89.508	102.167	89.85	9.741

Interlayer cation	Cell length			Cell angle			Illite layer thickness (Å)
Cs	a (Å)	b (Å)	c (Å)	α (degrees)	β (degrees)	γ (degrees)	
Substitution 1	10.402	8.979	10.585	89.784	101.317	89.82	10.379
Substitution 2	10.392	8.978	10.59	89.832	101.35	89.859	10.383

Generalised Gradient Approximation							
Interlayer cation	Cell length			Cell angle			Illite layer thickness (Å)
K	a (Å)	b (Å)	c (Å)	α (degrees)	β (degrees)	γ (degrees)	
Substitution 1	10.58	9.141	10.542	89.379	102.78	89.691	10.281
Substitution 2	10.598	9.127	10.519	89.321	102.527	89.718	10.268

Interlayer cation	Cell length			Cell angle			Illite layer thickness (Å)
Cs	a (Å)	b (Å)	c (Å)	α (degrees)	β (degrees)	γ (degrees)	
Substitution 1	10.626	9.174	11.199	89.599	101.261	89.86	10.984
Substitution 2	10.635	9.167	11.197	89.637	101.203	89.788	10.983

S6. EDX mapping

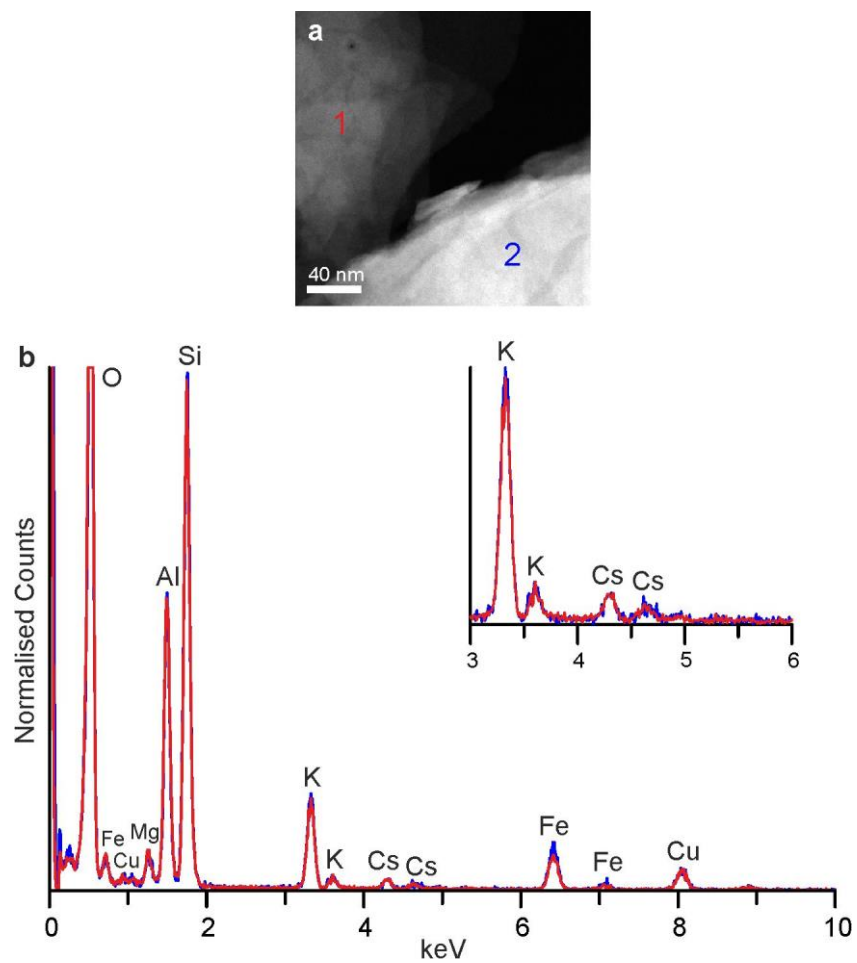


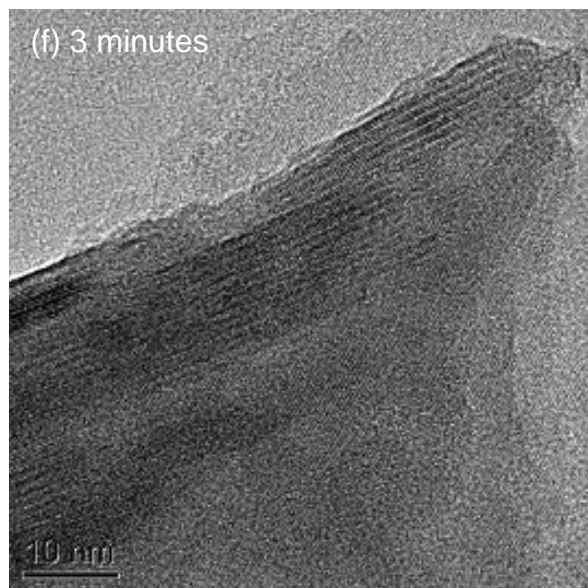
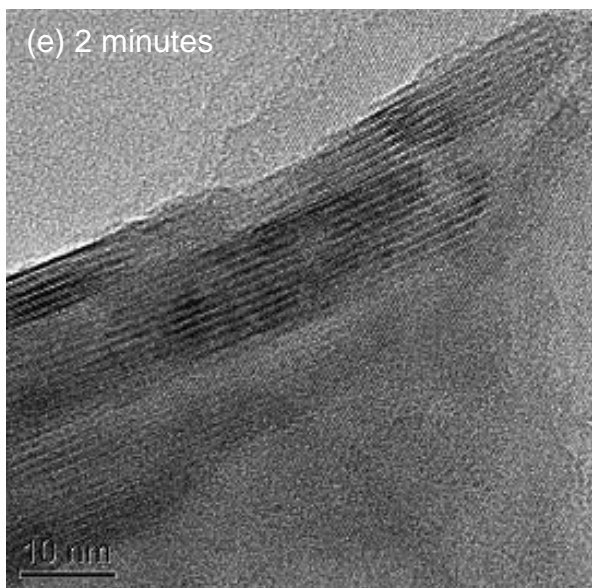
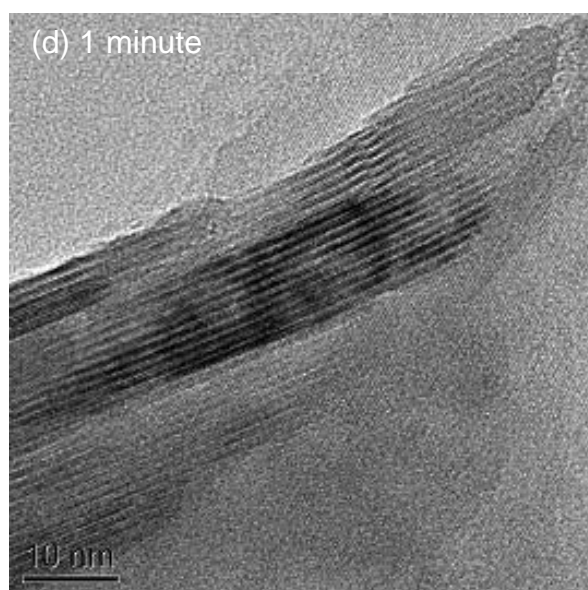
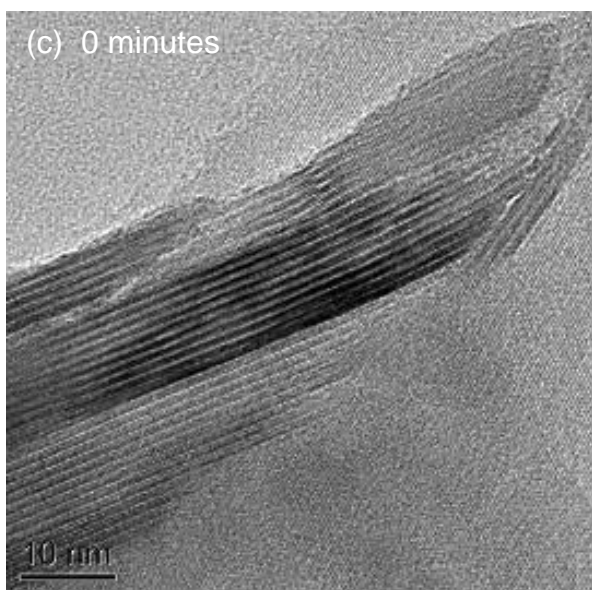
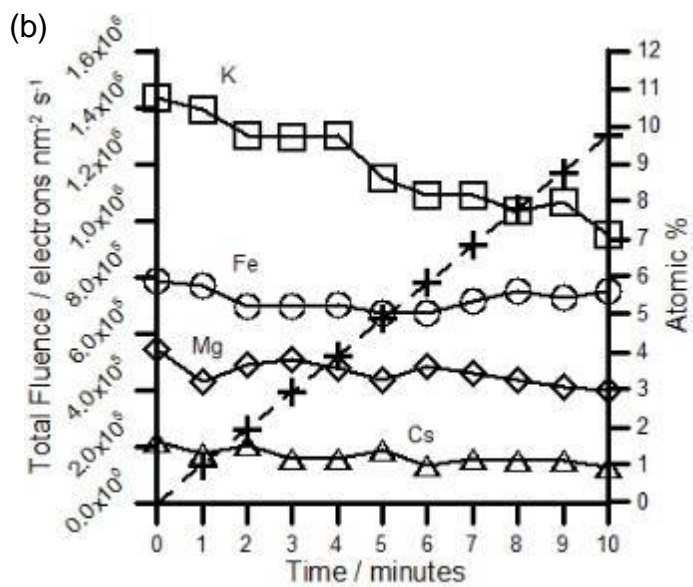
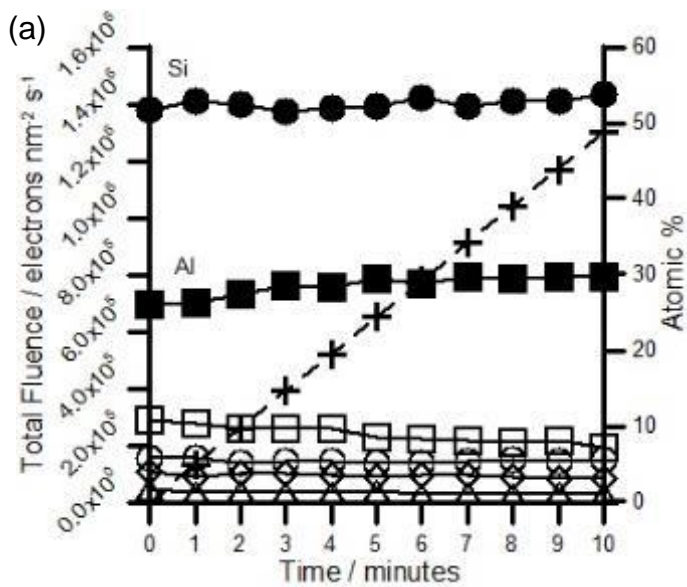
Figure S6 (a) EDX of mapped flakes shown in main text figure 3, (b) Normalised (on Si) EDX spectra from the two labelled flakes showing the same Cs and K composition unrelated to sample thickness

S7. Damage of illite by the TEM electron beam

When materials are exposed to an electron beam for a sufficient period of time they become damaged by the processes of radiolysis (or ionisation damage) and atom knock-on (Champness, 2001). Radiolysis dominates in insulating materials or semi-conductors (such as organics and silicate minerals) whilst conductive metals are resilient to radiolysis and primarily damage via knock-on effects (Egerton, 2013). Radiolysis occurs when the beam's high energy electrons collide with lower energy electrons orbiting the specimen atoms. The resulting transfer of energy raises the orbital electrons to higher energy levels and leaves a core hole (Egerton, 2013). In conductive materials (such as metals) electrons quickly migrate to fill this hole and the atomic bonds remain intact (Egerton, 2013). In insulating materials this ionisation disrupts atomic bonds and causes the material to become amorphous (Champness, 2001, Agar et al., 1974). Knock-on occurs when one of the beam's high energy electrons collides with the nucleus of a specimen atom (Egerton et al., 2010). The high energy electrons displace the atoms and they can then migrate within the sample (often clumping together) or be lost into the void (Champness, 2001, Cosslett, 1969).

Materials vary widely in their resistance to damage because of their conductivity, elemental composition and the strength of inter-atomic bonds. Clay minerals are easily damaged by radiolysis and knock-on effects (Kogure, 2002, Chi et al., 1998). Clays often become damaged after very short exposure time (<10 seconds) when imaged at high resolution, meaning images must be acquired very rapidly (Chen et al., 1997, Chen and Hayes, 1999).

Electron beam induced sample damage is more serious an issue for high resolution work due to higher current densities at the specimen. In order to better understand this damage process we performed a TEM imaging and EDX time series. Most TEM is performed at room temperature but imaging below room temperature has been proposed as a mechanism to reduce radiation damage (Cosslett, 1969). We therefore repeated our imaging and EDX time series both at room temperature (figure S7) and at -190°C (figure S8). We saw that cooling made little difference to the morphology observed during damage of the sample over 10 minutes, with both samples losing their crystallinity and becoming amorphous. However the loss of K during imaging was slower at cooler temperatures. This is likely to be the result of the reduced kinetic energy of the atoms at lower temperatures slowing their diffusion, meaning they migrated outside of the field of view more slowly and therefore continued to be detected by EDX even when the sample was amorphous. Our samples retained their crystallinity at this fluence rate for around one minute. But by two minutes significant damage was visible and by three minutes the samples were largely amorphous. It is not clear from these results whether damage is dominated by radiolysis or knock-on but it is likely that both processes are contributing. STEM imaging on the Titan was found to cause similar changes in the morphology of the samples but no systematic studies were undertaken for this imaging mode. Although beam induced radiation damage compromised the resolution of both the STEM images and the EDX spectrum images it did not prevent significant new findings being obtained to answer the project's hypothesis.



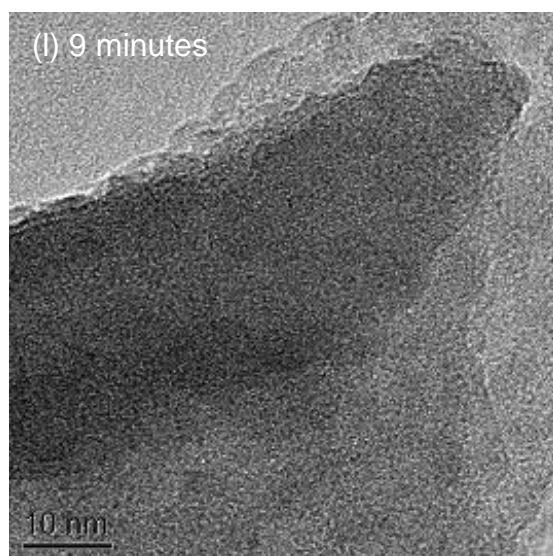
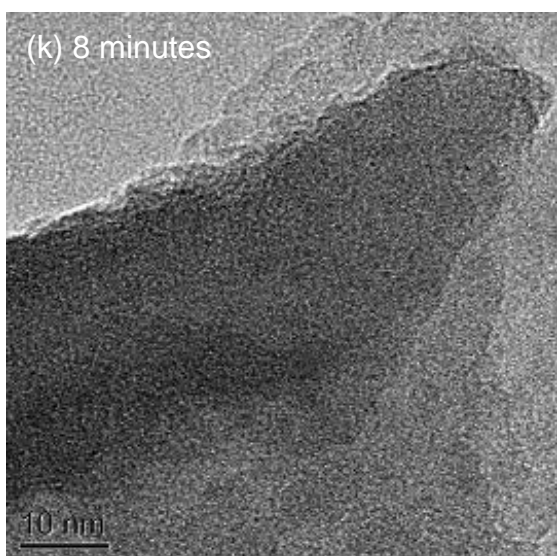
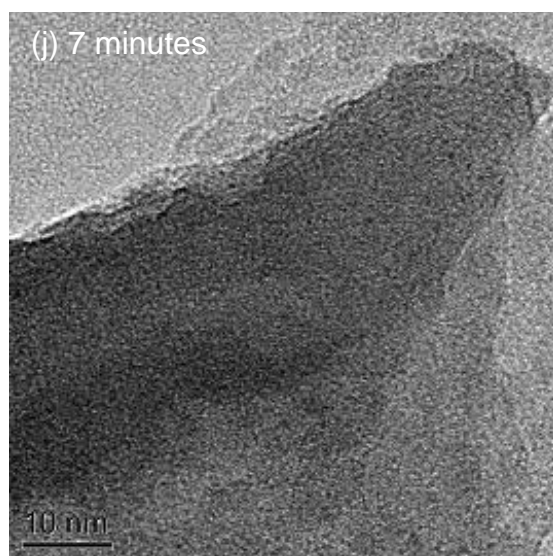
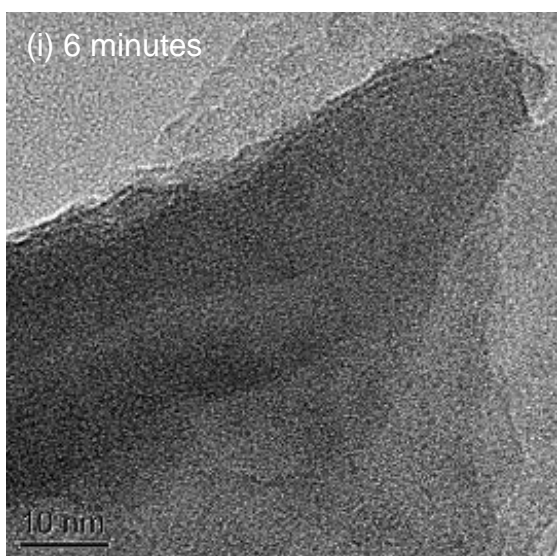
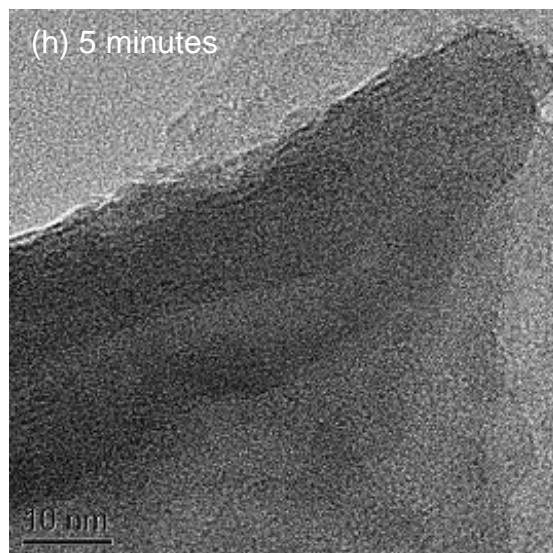
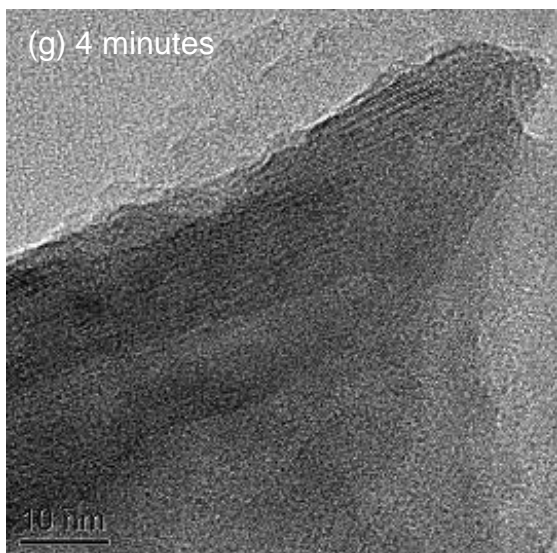
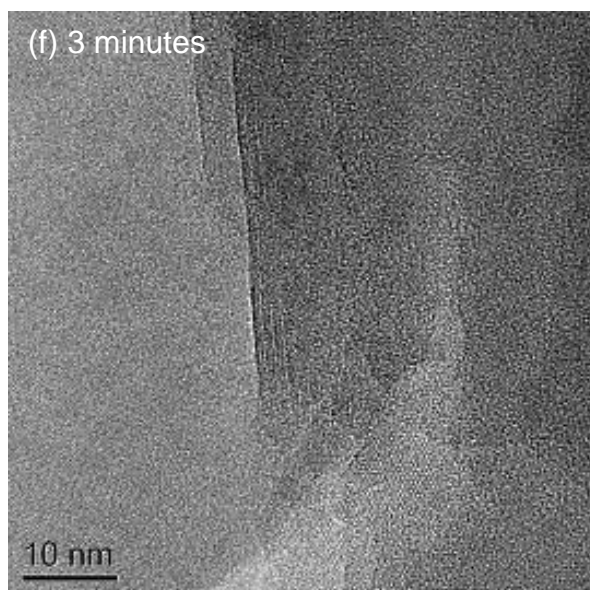
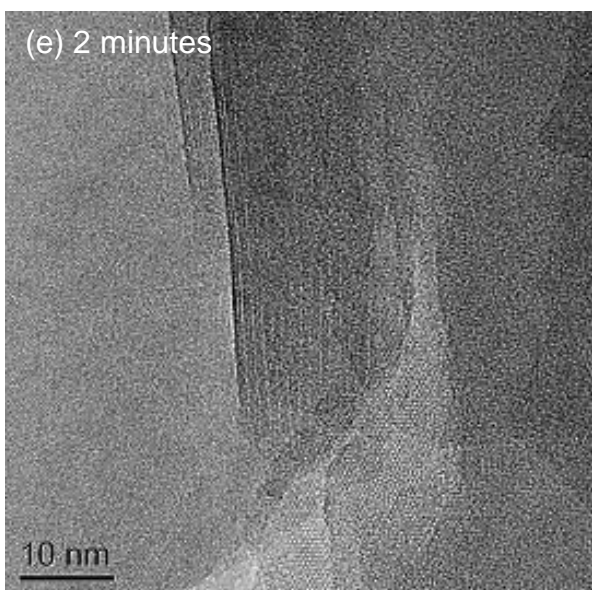
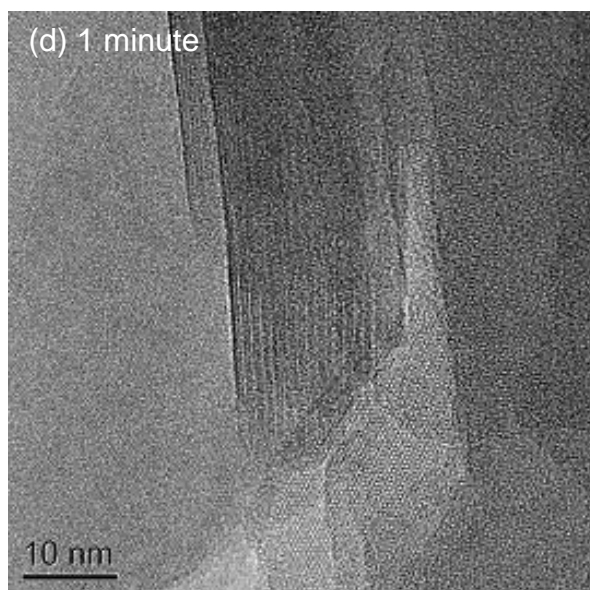
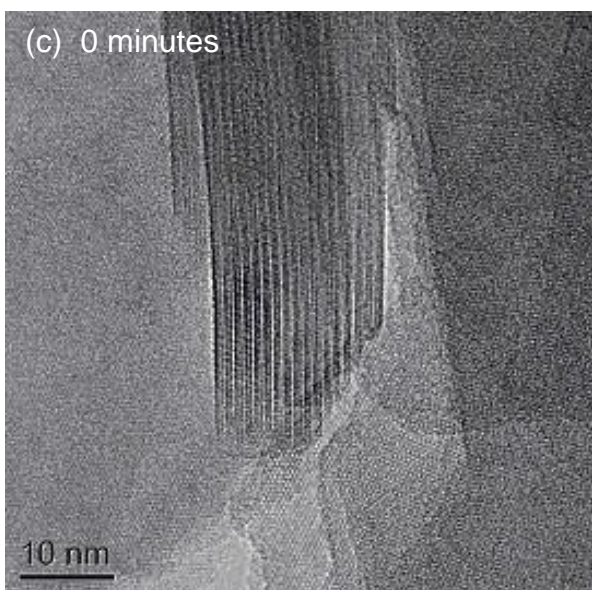
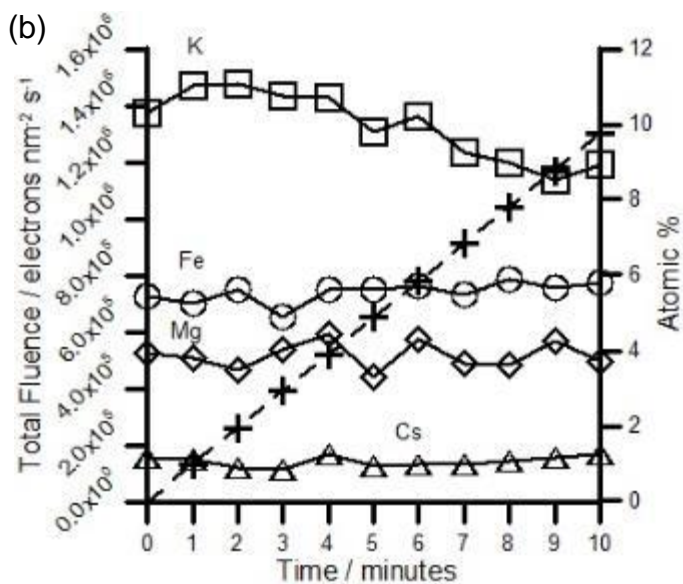
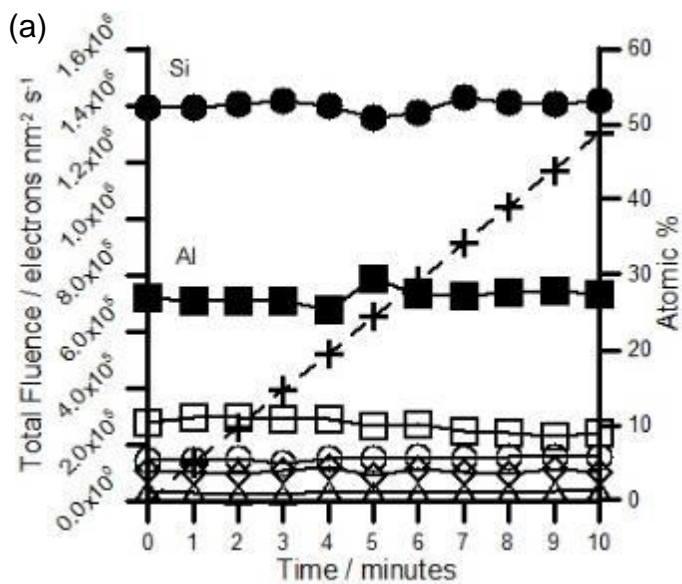


Figure S7 Time series of illite damage by the electron beam when imaged at 20°C. The graph (a) shows the reduction in relative atomic % of key atoms in the sample as a product of increasing electron fluence. Symbols show % of Si (solid circles) Al (solid squares), K (hollow squares), Fe (hollow circles), Mg (hollow diamonds) and Cs (hollow triangles). Graph (b) shows an expanded region of graph (a) with Si and Al removed. Image (c) shows the sample at the beginning of the imaging period and images (d-l) were taken every minute for a further 9 minutes to show loss of sample crystallinity.



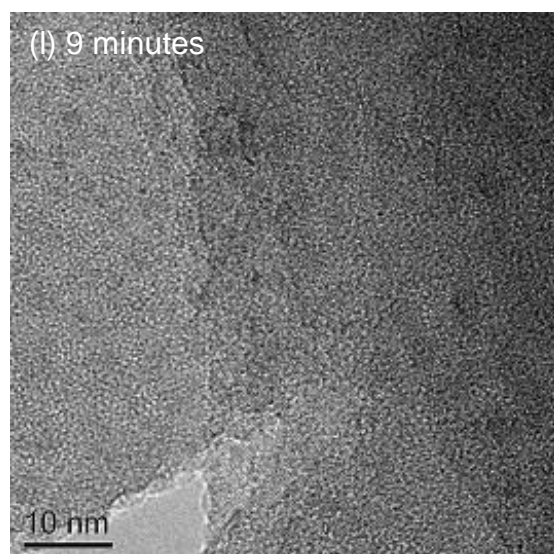
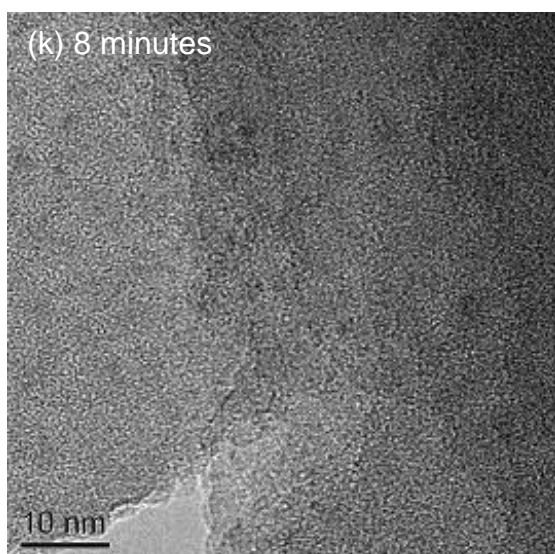
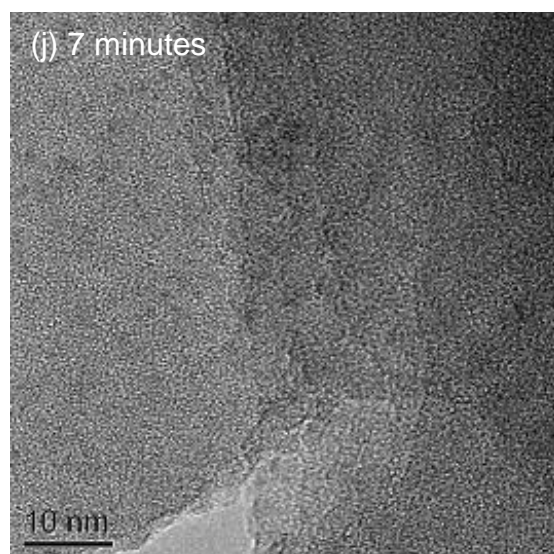
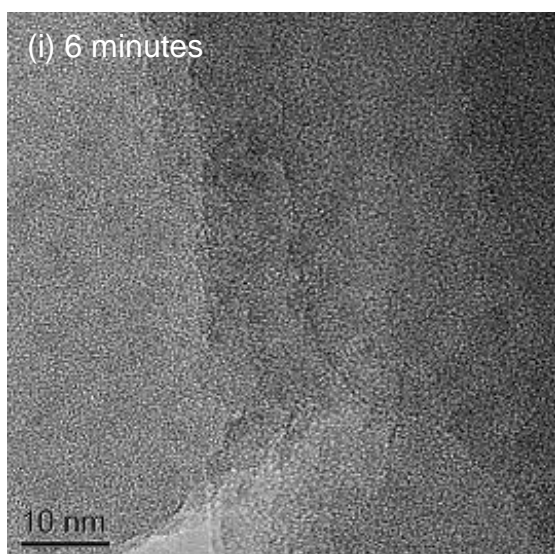
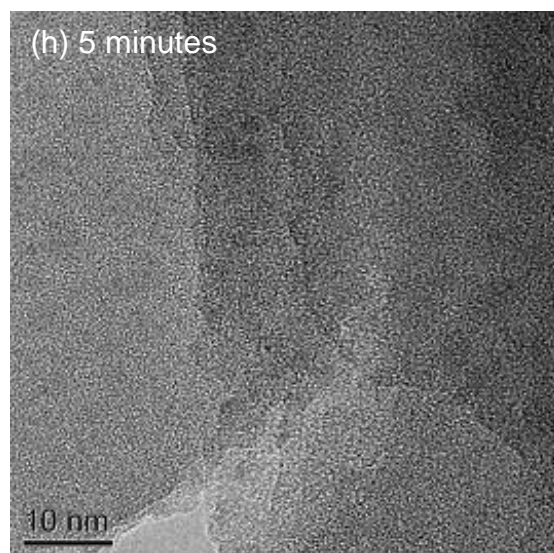
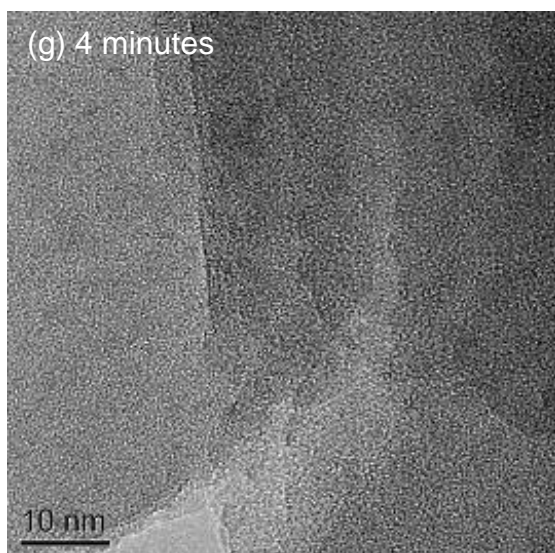


Figure S8 Time series of illite damage by the electron beam when imaged at -190°C . The graph (a) shows the reduction in relative atomic % of key atoms in the sample as a product of increasing electron fluence. Symbols show % of Si (solid circles) Al (solid squares), K (hollow squares), Fe (hollow circles), Mg (hollow diamonds) and Cs (hollow triangles). Graph (b) shows an expanded region of graph (a) with Si and Al removed. Image (c) shows the sample at the beginning of the imaging period and images (d-l) were taken every minute for a further 9 minutes to show loss of sample crystallinity.

S8. References

- Agar, A. W., Alderson, R. H. & Chescocoe, D. 1974. *Practical Methods in Electron Microscopy Volume 2: Principles and Practice of Electron Microscope Operation*, Amsterdam, North-Holland Publishing Company.
- Champness, P. E. 2001. *Electron Diffraction in the Transmission Electron Microscope*, Oxford, BIOS.
- Chen, C. C. & Hayes, K. F. 1999. X-ray absorption spectroscopy investigation of aqueous Co(II) and Sr(II) sorption at clay-water interfaces. *Geochimica Et Cosmochimica Acta*, 63, 3205-3215.
- Chen, C. C., Hayes, K. F. & Papelis, C. 1997. In-situ EXAFS study on aqueous cobalt(II) and strontium(II) sorption at clay-water interfaces as a function of various solution conditions. *Abstracts of Papers of the American Chemical Society*, 214, 48-GEOC.
- Chi, M., FitzGerald, J. D., Eggleton, R. A. & Llewellyn, D. J. 1998. Analytical electron microscopy in clays and other phyllosilicates: loss of elements from a 9-nm stationary beam of 300-keV electrons. *Clays and Clay Minerals*, 46, 301-316.
- Cosslett, V. E. 1969. High-Voltage Electron Microscopy. *Quarterly Reviews of Biophysics*, 2, 95-133.
- Egerton, R. F. 2013. Control of radiation damage in the TEM. *Ultramicroscopy*, 127, 100-108.
- Egerton, R. F., McLeod, R., Wang, F. & Malac, M. 2010. Basic questions related to electron-induced sputtering in the TEM. *Ultramicroscopy*, 110, 991-997.
- Kogure, T. 2002. Investigations of Micas Using Advanced Transmission Electron Microscopy. In: MOTTANA, A., PAOLO SASSI, F., THOMPSON JR, J. B. & GUGGENHEIM, S. (eds.) *Micas: Crystal Chemistry and Metamorphic Petrology*. Mineralogical Society of America.
- Perdew, J. P., Burke, K. & Ernzerhof, M. 1996. Generalized gradient approximation made simple. *Physical Review Letters*, 77, 3865-3868.
- Perdew, J. P. & Zunger, A. 1981. Self-interaction correction to density-functional approximations for many electron systems. *Physical Review A*, 23.